Heat Transfer Engineering

ISSN: 0145-7632 (Print) 1521-0537 (Online) Journal homepage: http://www.tandfonline.com/loi/uhte20

Improved Treatment of Anisotropic Scattering in Radiation Transfer Analysis Using the Finite Volume Method

Brian Hunter & Zhixiong Guo

To cite this article: Brian Hunter & Zhixiong Guo (2016) Improved Treatment of Anisotropic Scattering in Radiation Transfer Analysis Using the Finite Volume Method, Heat Transfer Engineering, 37:3-4, 341-350, DOI: 10.1080/15374416.2015.1052709

To link to this article: http://dx.doi.org/10.1080/15374416.2015.1052709

Accepted online: 01 Jun 2015.Published online: 26 Aug 2015.

Heat Transfer Engineering, 37(3–4):341–350, 2016

ISSN: 0145-7632 print / 1521-0537 online
DOI: 10.1080/15374416.2015.1052709

Improved Treatment of Anisotropic Scattering in Radiation Transfer Analysis Using the Finite Volume Method

BRIAN HUNTER and ZHIXIONG GUO

Department of Mechanical and Aerospace Engineering, Rutgers, The State University of New Jersey, Piscataway, New Jersey, USA

Discretization of the integral anisotropic-scattering term in the equation of radiative transfer will result in two kinds of numerical errors: alterations in scattered energy and asymmetry factor. Though quadrature flexibility with large angular directions and further solid-angle splitting in the finite volume method (FVM) allow for reduction/minimization of these errors, computational efficiency is adversely impacted. A phase-function normalization technique to get rid of these errors is simpler and is applied to the three-dimensional (3-D) FVM for the first time to improve anisotropic radiation transfer computation accuracy and efficiency. FVM results are compared to Monte Carlo and discrete-ordinates method predictions of radiative heat transfer in a cubic enclosure housing a highly anisotropic participating medium. It is found that the FVM results generated using the normalization technique conform accurately to the results of the other two methods with little impact on computational efficiency.

INTRODUCTION

In engineering problems where radiation is the dominant mode of heat transfer, such as high-temperature combustion and material processing [1–5], fire and solar radiation [6–8], and laser applications [9–12], accurate solutions of the equation of radiative transfer (ERT) are required for full radiation characterization. The integro-differential nature of the ERT makes analytical solution difficult, and thus numerical methods, such as the finite volume method (FVM) and discrete-ordinates method (DOM), are preferred.

The FVM was introduced as a method of predicting radiation heat transfer in the early 1990s [13–16]. Raithby [17] presented an excellent discussion of the FVM in two-dimensional (2-D) and three-dimensional (3-D) enclosures with unstructured grids. Chai et al. [18] analyzed ultrafast radiation heat transfer in a 3-D rectangular medium using the FVM, expanding on an earlier similar analysis using the DOM [19]. Kim and Huh [20] introduced a new angular discretization scheme for the FVM.

In practical applications, radiation scattering is anisotropic. In all discretization-based numerical methods, including FVM and DOM, the continuous angular variation of radiation scattering is approximated using a finite number of discrete radiation directions. A well-known issue for anisotropic-scattering media is that scattered energy becomes nonconserved after directional discretization [21]. This issue can be corrected using phase-function normalization in DOM [21–26]. For the FVM, scattered energy may be conserved using a solid-angle splitting technique [14]. A less known issue is the alteration in phase-function asymmetry factor [22–27] for both FVM and DOM, resulting in an error termed "angular false scattering."

Recently, Hunter and Guo [22] developed a phase-function normalization technique to simultaneously conserve scattered energy and phase-function asymmetry factor after directional discretization. The impact of this normalization on angular false-scattering errors was analyzed for 2-D axisymmetric [22, 23] and 3-D cubic enclosures [24, 25] using the DOM, where DOM predictions were vastly improved in comparison to benchmark Monte Carlo (MC) results. Hunter and Guo [27] found that

Address correspondence to Professor Zhixiong Guo, Department of Mechanical and Aerospace Engineering, Rutgers, The State University of New Jersey, 98 Brett Road, Piscataway, NJ 08854, USA. E-mail: guo@jove.rutgers.edu

Color versions of one or more of the figures in the article can be found online at www.tandfonline.com/uhte.

angular false scattering still persisted after FVM discretization even with substantial refinement in solid-angle splitting in 2-D axisymmetric cylindrical enclosures. As most practical applications cannot be approximated as two-dimensional, it is necessary to investigate angular false-scattering errors for 3-D FVM.

In this study, radiation transfer in a 3-D cubic enclosure containing an anisotropic-scattering medium is predicted using the FVM. The necessity of using the authors' phase-function normalization technique to ensure minimization of angular false scattering and improve treatment of anisotropic scattering in radiation transfer analysis is presented. Heat fluxes generated using the FVM both with and without phase-function normalization are compared to MC [26] and DOM results [25] to gauge the accuracy of the FVM predictions. The impact of solid-angle splitting on both scattered energy and asymmetry factor conservation is analyzed. A discussion on the computational advantages of using phase-function normalization is presented.

THE FINITE VOLUME METHOD

The steady-state ERT of radiation intensity I in a gray, absorbing–emitting and anisotropically scattering medium can be expressed, using general vector notation, as follows:

$$\hat{s}\cdot\nabla I(\boldsymbol{r},\hat{\boldsymbol{s}}) = -(\sigma_a+\sigma_s)I(\boldsymbol{r},\hat{\boldsymbol{s}}) + \sigma_a I_b(\boldsymbol{r}) + \frac{\sigma_s}{4\pi}\oint\!\!\!\!\!\!\iint_{4\pi} I(\boldsymbol{r},\hat{\boldsymbol{s}}')\Phi(\hat{\boldsymbol{s}}',\hat{\boldsymbol{s}})d\Omega' \tag{1}$$

In the preceding equation, the term on the left-hand side accounts for spatial gradients of radiative intensity, while the three right-hand-side terms represent intensity attenuation due to both absorption and radiative out-scattering, intensity augmentation due to medium emission, and intensity augmentation due to in-scattering of radiative energy, respectively.

Using a control-volume approach, Eq. (1) is integrated over control volume ΔV and discrete solid angle $\Delta\Omega^l$ [16], defined by azimuthal angle ϕ and polar angle θ, where the discrete radiation direction $\hat{s}^l$ denotes the centroid of $\Delta\Omega^l$ [15, 16]. After performing the integration and evaluating the integrals over control volume and solid angle, the discretized form of Eq. (1) can be expressed as follows:

$$\sum_i I_i^l A_i D_i^l = -(\sigma_a+\sigma_s)I^l\Delta V\Delta\Omega^l + S^l\Delta V\Delta\Omega^l,\ l=1,2,\ldots,M \tag{2}$$

where M is the total number of discrete radiation directions $\hat{s}^l$. In this summation, I_i^l represents radiative intensity in discrete direction $\hat{s}^l$ at control-volume face i, A_i is the facial surface area of control-volume face i, and D_i^l is the directional weight of discrete direction $\hat{s}^l$ at control-volume face i, evaluated using the following expression:

$$D_i^l = \iint_{\Delta\Omega^l}(\hat{\boldsymbol{s}}^l\cdot\hat{\boldsymbol{n}}_i)d\Omega^l \tag{3}$$

where $\hat{\boldsymbol{n}}_i$ is the unit vector normal to control-volume face i.

The source term S^l can be expressed as

$$S^l = \sigma_a I_b + \frac{\sigma_s}{4\pi}\sum_{l'=1}^{M}\bar{\Phi}^{l'l}I^{l'}\Delta\Omega^{l'} \tag{4}$$

where the radiative in-scattering integral in Eq. (1) has been approximated using a discrete quadrature summation. In this summation, $\bar{\Phi}^{l'l}$ is the average scattering phase function between two discrete solid angles $\Delta\Omega^{l'}$ and $\Delta\Omega^l$, which can be calculated as such:

$$\bar{\Phi}^{l'l} = \frac{1}{\Delta\Omega^{l'}\Delta\Omega^l}\iint_{\Delta\Omega^l}\iint_{\Delta\Omega^{l'}}\Phi(\hat{\boldsymbol{s}}',\hat{\boldsymbol{s}})d\Omega' d\Omega \tag{5}$$

The necessity of using an averaged scattering phase function will be described later.

The choice of directions for the FVM is generally arbitrary. Commonly, the total solid angle of 4π is approximated using $M = (N_\phi \times N_\theta)$ discrete directions, where N_ϕ and N_θ are the number of divisions in the azimuthal and polar angle, respectively. However, Kim and Huh [20] discovered that for 3-D problems, angular discretization in this manner resulted in highly nonuniform solid angles. Thus, they introduced a new angular discretization method for the FVM called the FT_N-FVM. Using this method, the total polar angle θ is divided into an even number N of uniformly spaced directional levels. The number of azimuthal divisions corresponding to the N polar levels follows the arithmetic sequence $4, 8, 12, \ldots 2N-4, 2N, 2N-4, \ldots, 12, 8, 4$. The total number of directions becomes $M = N(N+2)$. Kim and Huh [20] showed that this procedure produces more uniform solid angles, leading to improvement in radiation transfer results over the commonly used $(N_\phi \times N_\theta)$ angular discretization. To this end, the FT_N-FVM discretization procedure is implemented for all forthcoming results in this analysis.

Additional details on the discretization of the ERT and solution procedure using the FVM are not presented here, for brevity, but are available in a textbook [1] and in the authors' recent publications [23, 28].

PHASE FUNCTION NORMALIZATION

It is well established that discretization of the angular variation must conserve scattered energy for all discrete directions $\hat{s}^{l'}$:

$$\frac{1}{4\pi}\sum_{l=1}^{M}\Phi^{l'l}\Delta\Omega^l = 1 \tag{6}$$

If scattering is isotropic, the preceding condition is explicitly satisfied. However, radiation scattering is always anisotropic in natural materials and the preceding conservation is usually broken when anisotropy is considered [14]. Inaccurate conservation of scattered energy has been shown to produce inaccurate radiation transfer predictions [26].

To correct this issue, Chui et al. [14] introduced a solid-angle splitting technique, in which each solid angle $\Delta\Omega^{l}$ is subdivided into multiple subangles $\Delta\Omega^{l_s}$. The total scattered energy between any two arbitrary solid angles isthen calculated by averaging the energy scattered between their corresponding sub-angles. Using this technique, the average scattering phase function of Eq. (5) can be approximated as follows [13]:

$$\bar{\Phi}^{l'l} \cong \frac{1}{\Delta\Omega^{l'}\Delta\Omega^{l}} \sum_{l_s=1}^{M_s} \sum_{l'_s=1}^{M'_s} \Phi^{l'_s l_s} \Delta\Omega^{l'_s} \Delta\Omega^{l_s} \tag{7}$$

In the preceding equation, $\Phi^{l'_s l_s}$ is the discrete scattering phase function between subangles $\Delta\Omega^{l'_s}$ and $\Delta\Omega^{l_s}$, and M_s and M'_s are the number of total subangles in solid angles $\Delta\Omega^{l}$ and $\Delta\Omega^{l'}$, respectively. After averaging, the scattered energy conservation of Eq. (6) becomes

$$\frac{1}{4\pi} \sum_{l=1}^{M} \bar{\Phi}^{l'l} \Delta\Omega^{l} = 1 \tag{8}$$

Assuming every solid angle is divided into a sufficient number of subangles, this conservation condition will be accurately satisfied for all directions $\hat{s}^{l'}$, regardless of phase-function type.

In order to ease numerical computation, approximations to the highly oscillatory Mie phase function Φ are commonly implemented, as the physical nature of Φ makes it difficult to efficiently adopt it. For highly anisotropic scattering, the Henyey–Greenstein (HG) phase function is widely accepted as a suitable approximation, due to its accurate representation of the strong forward-scattering peak [1]. The HG phase function approximation can be expressed as

$$\Phi_{HG}(\Theta) = \sum_{n=0}^{\infty} (2n+1)\, g^n P_n(\cos\Theta)$$

$$= \frac{1-g^2}{\left[1+g^2-2g\cos\Theta\right]^{1.5}} \tag{9}$$

where Θ is the scattering angle between incoming and outgoing radiation directions, $P_n$is the nth-order Legendre polynomial, and the phase-function asymmetry factor g is the average cosine of scattering angle.

Figure 1 illustrates the dependence of scattered energy conservation on the number of solid-angle splitting after FVM discretization for HG phase function approximation with g = 0.9300. The continuous angular variation is discretized using M = 24, 48, 80, 168, and 288 discrete directions. Each solid angle is subdivided into $(N_{s\phi} \times N_{s\theta})$ subangles, with $N_{s\phi} = N_{s\theta}$, ranging from (2 × 2) to (24 × 24) divisions. For a given number of discrete directions, increases in the number of subangles reduce the discrepancy in discretized scattered energy conservation. In order to conserve scattered energy accurately within 0.001%, $(N_{s\phi} \times N_{s\theta})$ = (24 × 24), (20 × 20), (20 × 20), (12 × 12), and (12 × 12) subangles are required for M =24, 48, 80, 168, and 288, respectively. Sufficient solid-angle splitting may accurately conserve scattered energy.

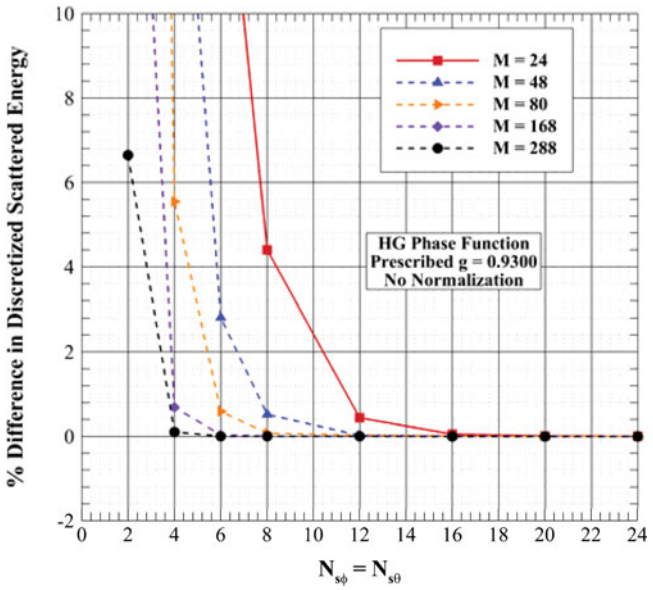

Figure 1 Deviation from scattered energy conservation versus solid-angle splitting number for HG phase function with g = 0.9300 with various angular quadratures.

In addition to scattered energy, the overall phase-function asymmetry factor g should also be conserved after directional discretization [22]. Thus, the following relation should hold for all discrete directions $\hat{s}^{l'}$:

$$\frac{1}{4\pi} \sum_{l=1}^{M} \bar{\Phi}^{l'l} \cos\Theta^{l'l} \Delta\Omega^{l} = g \tag{10}$$

where $\Theta^{l'l}$ is the scattering angle between incoming direction $\hat{\mathbf{s}}^{l'}$ and scattered direction $\hat{\mathbf{s}}^{l}$.

Figure 2 illustrates the deviation from asymmetry factor conservation for the same conditions as Figure 1. The behaviors are quite different from Figure 1. When solid-angle splitting level is initially increased, the discretized asymmetry factor value will converge toward its prescribed value (g = 0.9300); however, the situation will worsen with further increase of splitting level after passing the convergence. At a very high splitting level of $(N_{s\phi} \times N_{s\theta})$ = (24 × 24), the discretized asymmetry factor for M = 24, 48, 80, 168, and 288 attains a value of 0.8855, 0.9024, 0.9113, 0.9198, and 0.9237, respectively. This discrepancy between prescribed and discretized asymmetry factor in the FVM had gone largely unnoticed, as the commonly implemented solid-angle splitting technique was assumed to accurately conserve the asymmetry factor [26] as well as scattered energy. Small errors in discretized asymmetry factor can produce significant errors in radiation transfer predictions. Errors of

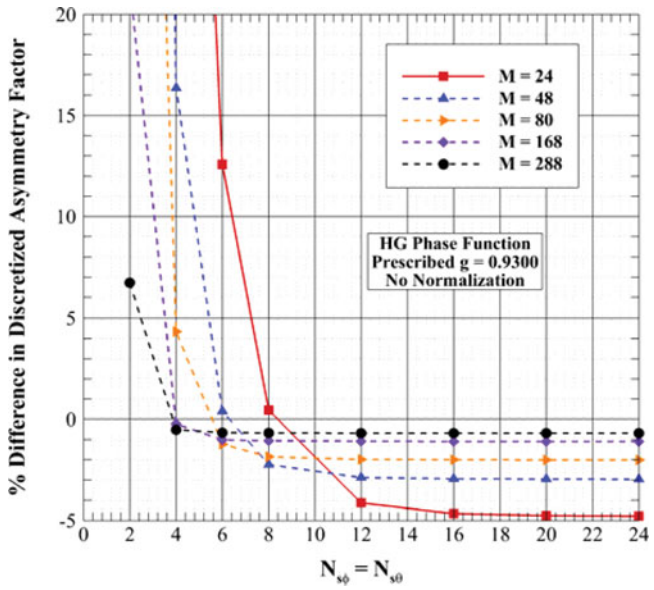

Figure 2 Deviation from asymmetry factor conservation versus solid-angle splitting number for HG phase function with g = 0.9300 with various angular quadratures.

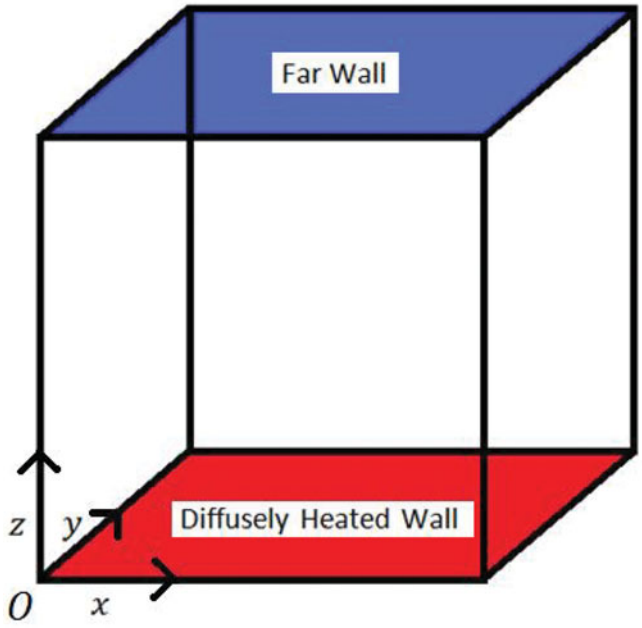

Figure 3 A cubic enclosure with coordinates.

this type are really false scattering due to angular discretization, or termed "angular false scattering" [24, 25].

To accurately conserve both scattered energy and asymmetry factor simultaneously, the average scattering phase function is normalized in the following manner [22]:

$$\tilde{\Phi}^{l'l} = \left(1 + A^{l'l}\right) \bar{\Phi}^{l'l} \tag{11}$$

where the normalization parameter $A^{l'l}$ corresponds to scattering between two discrete directions $\hat{\mathbf{s}}^{l'}$ and $\hat{\mathbf{s}}^{l}$. Normalization parameters $A^{l'l}$ are determined such that $\tilde{\Phi}^{l'l}$ satisfies Eqs. (8) and (10), as well as directional symmetry ($\tilde{\Phi}^{l'l} = \tilde{\Phi}^{ll'}$). Values of normalization matrix $A^{l'l}$ that will accurately conserve scattered energy as well as asymmetry factor after FVM discretization can be determined using pseudo-inversion.

RESULTS AND DISCUSSION

The benchmark test problem involves radiation heat transfer in a cubic participating enclosure of edge length L shown in Figure 3. The spatial coordinates are nondimensionalized as follows: $x^* = x/L$, $y^* = y/L$, and $z^* = z/L$. The optical thickness and scattering albedo of the medium are $\tau = (\sigma_a + \sigma_s)L$ and $\omega = \sigma_s/(\sigma_a + \sigma_s)$. Unless otherwise specified, the medium is taken to be cold ($I_b = 0$) and purely scattering ($\omega = 1.0$) with an optical thickness $\tau = 10.0$. All boundary walls are black, with the wall at $z^* = 0$ taken as a diffuse emitter with unity emissive power, and all remaining walls are taken to be cold. In order to relate the intensities at control-volume nodes to that of the control-volume faces in the FVM solution scheme, the positive spatial differencing scheme is used. For all simulations, a staggered spatial control-volume grid of $(N_x \times N_y \times N_z) = (27 \times 27 \times 27)$ with uniform grid steps of $\Delta x^* = \Delta y^* = \Delta z^* = 0.04$ is implemented, in order to minimize spatial discretization error.

The computing workstation used is a Dell Optiplex 780, with an Intel 2 Dual Core 3.16 GHz processor and 4.0 GB of RAM. The FVM procedure was implemented using the FORTRAN computing language, and the values of the normalization parameters were determined by using MATLAB, and imported into FORTRAN.

Figure 4 examines the impact of phase-function normalization on heat flux $Q(x^*, y^* = 0.5, z^* = 1.0)$ for three representative HG asymmetry factors: $g = 0.2000$, 0.8000, and

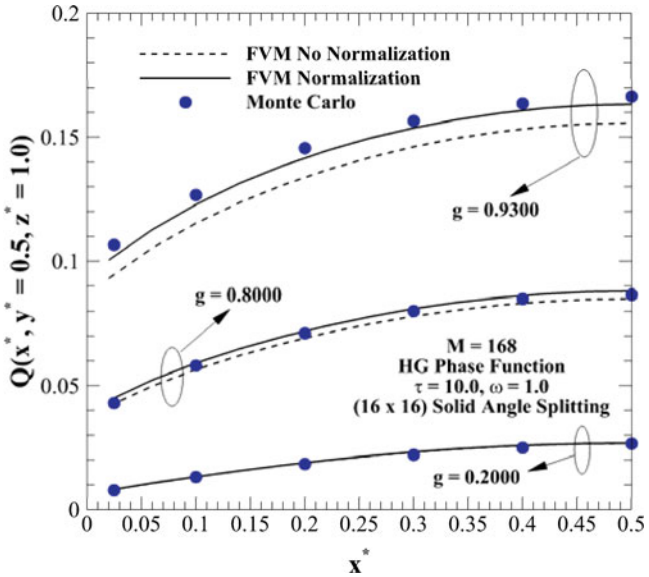

Figure 4 Impact of phase-function normalization on $Q(x^*, y^* = 0.5, z^* = 1)$ generated using FVM with $M = 168$ for $g = 0.9300$ and comparison with MC solutions [26].

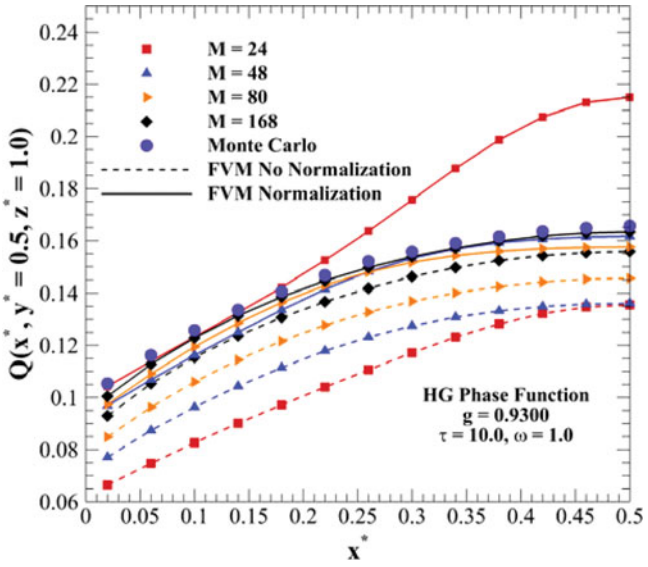

Figure 5 Impact of discrete direction number on $Q(x^*, y^* = 0.5, z^* = 1)$ and comparison with MC results [26] for g = 0.9300.

0.9300. Profiles generated via the FVM using either Hunter and Guo's normalization technique or no normalization with sufficient solid-angle splitting are compared to reference MC results [26]. The FVM profiles were generated using $M = 168$ discrete directions, and thus solid-angle splitting of $(N_{s\phi} \times N_{s\theta}) = (16 \times 16)$ is implemented so that scattered energy is conserved even without phase-function normalization. For weakly forward scattering ($g = 0.2000$), FVM profiles both with and without phase-function normalization produce nearly identical results. As asymmetry factor is increased to $g = 0.8000$, nonnormalization leads to a 5% change in scaled scattering effect $(1 - g)$. For the highly anisotropic case, the discretized g is altered from 0.9300 to 0.9198 (14.6% scaled scattering effect change). When compared to MC predictions, heat fluxes generated using normalization conform more accurately than when normalization is ignored. Without normalization, the FVM profile even with a large number of solid-angle splitting underpredicts the MC by 10%.

Figure 5 investigates the impact of angular discretization on both normalized and non-normalized FVM heat flux in a highly-anisotropic medium with $g = 0.9300$. Reference MC values are also plotted, for comparison. Solid angle splitting of (24×24) for $M = 24$, (20×20) for $M = 48$ and 80, and (16×16) for $M = 168$ is applied to both normalized and nonnormalized profiles, in order to accurately conserve scattered energy even without normalization. It is seen that normalization is much more efficient than increasing the angular directions in reducing the angular false-scattering errors. When normalization is applied, the differences between FVM and MC are dramatically reduced. One exception exists for the lowest directional order $M = 24$, where a difference of near 30% is still witnessed near the wall center.

The underlying cause of this large discrepancy may be found by examining the distribution of discretized phase function versus the cosine of scattering angle in comparison with the theoretical HG phase function values calculated using Eq. (9).

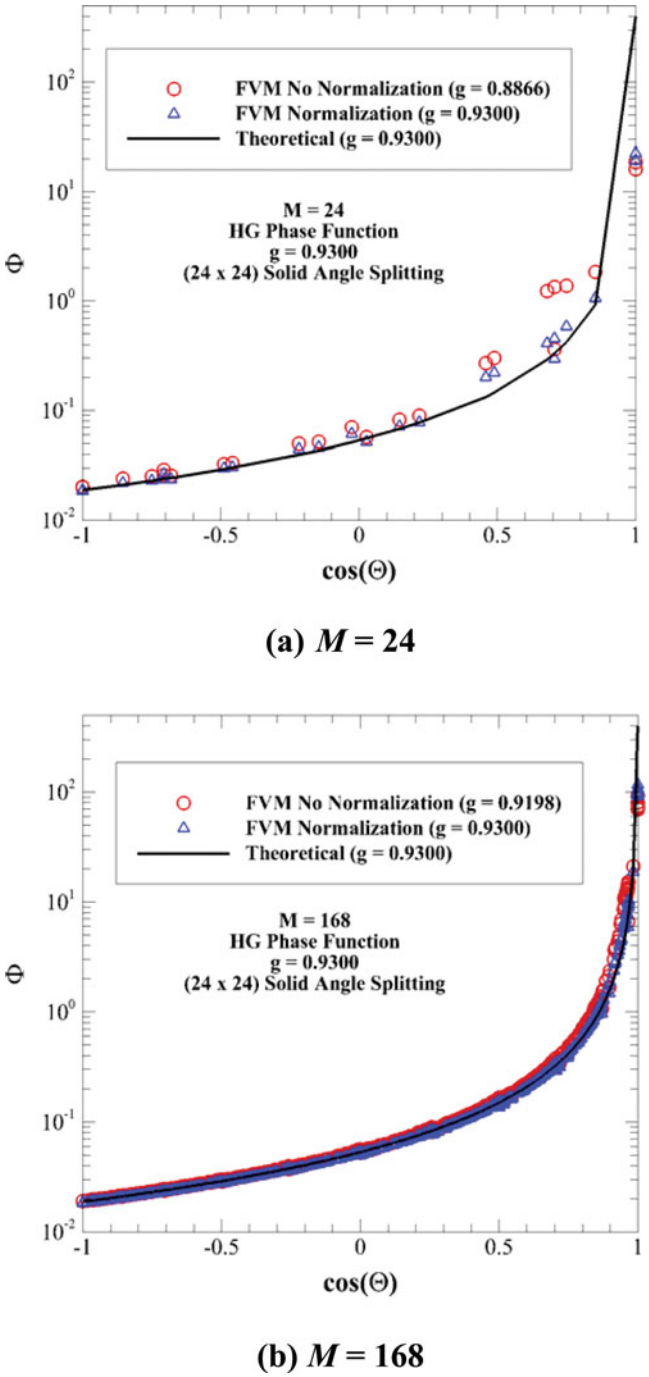

Figure 6 Comparison of discretized HG phase-function values vs. cosine of scattering angle with prescribed $g = 0.9300$ both with and without phase-function normalization using FVM with a) $M = 24$ and b) $M = 168$.

As shown in Figure 6a for $M = 24$, although asymmetry factor is effectively conserved after phase-function normalization, the discretized values of scattering phase function still exhibit some differences from the theoretical phase function values. The minimal amount of discrete directions $M = 24$ in the lowest quadrature isn't able to accurately represent the true nature of the theoretical phase function shape. In contrast, when an intermediate number of discrete directions is implemented, for

Table 1 Comparison of $Q(x^*, y^* = 0.5, z^* = 1.0)$ values generated using normalized DOM [25] and FVM to MC values [26] for a 3-D cube with $\tau = 10$, $\omega = 1$, and $g = 0.93$

		DOM	FVM	
x/L	MC	Normalization	No Normalization	Normalization
0.02	0.1053	0.0988	0.0930	0.1005
0.10	0.1258	0.1182	0.1153	0.1229
0.14	0.1336	0.1268	0.1237	0.1314
0.22	0.1467	0.1409	0.1368	0.1446
0.30	0.1557	0.1497	0.1461	0.1537
0.38	0.1615	0.1543	0.1523	0.1598
0.42	0.1635	0.1555	0.1542	0.1617
0.50	0.1656	0.1565	0.1558	0.1633

example, $M = 168$ as shown in Figure 6b, both asymmetry factor and phase-function shape are preserved after normalization.

A comparison of heat flux profile $Q(x^*, y^* = 0.5, z^* = 1.0)$ generated using the FVM both with and without phase-function normalization to both MC [26] and DOM S_{12} [25] results is presented in Table 1. For DOM, there is no way to implement an analogous solid-angle splitting technique, so phase-function normalization is always required for anisotropic scattering radiation transfer. Both DOM and FVM adopt the same spatial grid, that is, $(N_x \times N_y \times N_z) = (27 \times 27 \times 27)$, and have the same directional number $M = 168$. Solid-angle splitting of (24×24) is used in the FVM. Results should be similar among the three solution methods if they are accurate. Heat fluxes generated using the DOM S_{12} with Hunter and Guo's normalization technique, which accurately preserves the prescribed g value, result in differences of $<7\%$ at all locations in comparison to MC. Sufficient solid-angle splitting in FVM to conserve scattered energy produces a discretized $g = 0.9198$ without normalization, resulting in underpredictions up to 12% as compared with MC. Application of normalization in the FVM accurately preserves the prescribed g value and reduces the error to $<5\%$ at maximum. The average difference between DOM and FVM with normalization is only 3%. The accurate conformity of normalized FVM to both MC and normalized DOM results gives confidence that anisotropic scattering properties of the medium are being accurately accounted for through proper phase-function normalization.

The impact of solid-angle splitting on radiation heat flux results generated using the FVM both with and without normalization is examined in Figures 7a and 7b for $M = 80$ and 288, respectively, in which percentage differences between FVM heat fluxes and reference MC results are plotted for various levels of solid-angle splitting. As discussed in the results shown in Figure 1, solid-angle splitting of $(N_{s\phi} \times N_{s\theta}) = (20 \times 20)$ and (12×12) are required to accurately conserve scattered energy within 0.001% for $M = 80$ and 288, respectively. As seen in Figure 7, there exist large heat flux percentage differences when normalization is ignored for these two cases. Increasing the splitting level to (24×24), the discrepancies between MC and FVM results without normalization are still large. However, the differences between normalized FVM and MC are very small, even with use of the lowest splitting level of (2×2). FVM profiles with normalization generated with both lowest (2×2) and high splitting (24×24) densities are nearly identical. This indicates that further solid-angle splitting past (2×2) is not required to obtain more accurate radiation transfer solutions when implementing normalization.

The ability to produce accurate FVM solutions with minimal solid-angle splitting and low-order directional quadrature has a distinct advantage when it comes to computational convergence time in addition to memory requirement. FVM convergence times for varying number of discrete directions and various solid angle splitting levels are presented in Table 2 for the problem analyzed in Figure 5. Computational times for

Table 2 Computational convergence times, in seconds, for FVM with and without normalization at various solid-angle splitting levels and varying number of discrete directions

	No Normalization								Normalization
M\(Nsϕ × Nsθ)	(2 × 2)	(4 × 4)	(6 × 6)	(8 × 8)	(12 × 12)	(16 × 16)	(20 × 20)	(24 × 24)	(2 × 2)
24	Diverge	Diverge	21.37	14.70	15.38	20.76	33.03	50.86	14.51
48	Diverge	75.21	50.00	47.21	54.40	77.532	124.0	207.0	41.84
80	Diverge	116.5	110.6	113.0	141.8	203.9	335.9	556.6	109.8
168	Diverge	531.0	491.5	514.1	606.7	834.2	1415	2414	497.0
288	1538	1385	1340	1438	1687	2438	4133	7011	1341

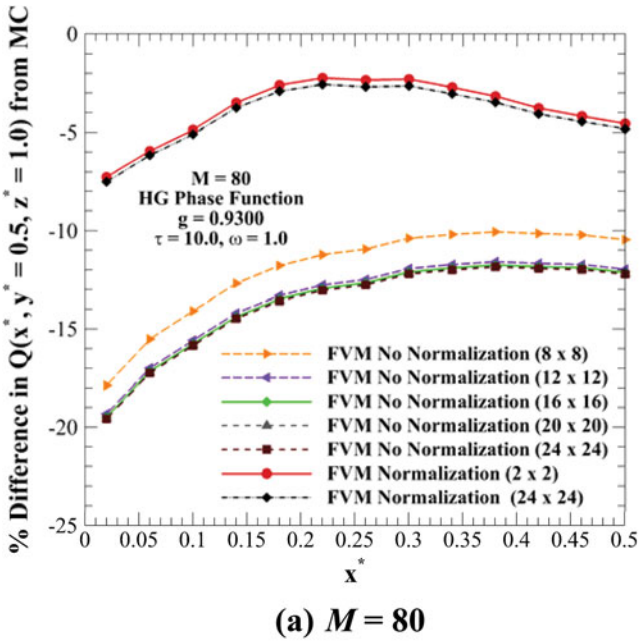

(a) $M = 80$

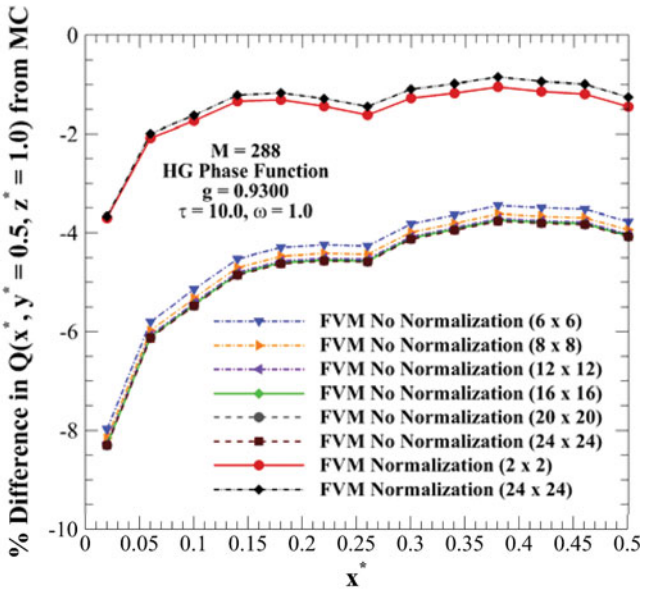

(b) $M = 288$

Figure 7 Percent difference in $Q(x^*, y^* = 0.5, z^* = 1)$ between MC solution [26] and FVM solutions both with and without phase-function normalization using various solid angle splitting densities for a) $M = 80$ and b) $M = 288$.

$M = 24$ to 288 using splitting levels ranging from $(N_{s\phi} \times N_{s\theta}) = (2 \times 2)$ to (24×24) for the nonnormalized case are presented, as well as the corresponding computational times for normalization with $\left(N_{s\phi} \times N_{s\theta}\right) = (2 \times 2)$ splitting. When normalization is not applied, (2×2) solid-angle splitting results in divergent radiation transfer solutions for all directional quadratures except $M = 288$. In general, refinement of solid-angle splitting leads to substantial increases in computational time. For $M = 288$, increasing splitting level from (4×4) to (24×24) results in a 406% increase in computational time. Use of normalization allows for convergence and accuracy with just (2×2) splitting and relatively low-order quadrature, reducing computational times substantially.

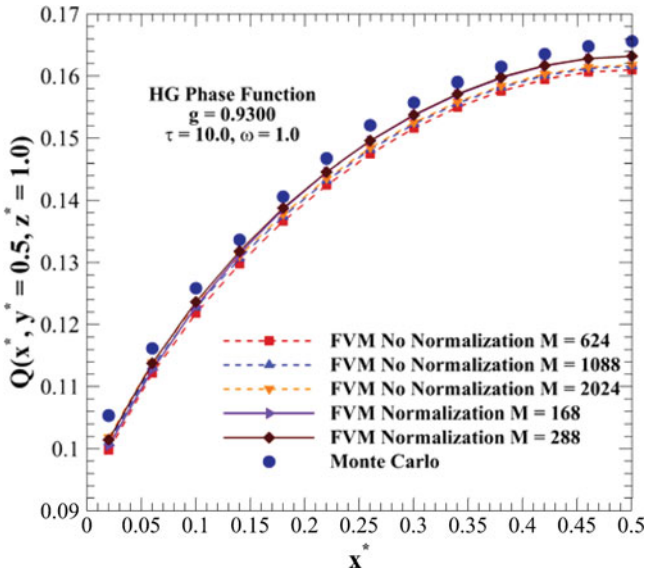

Figure 8 Comparison of $Q(x^*, y^* = 0.5, z^* = 1.0)$ between MC solutions [26] and FVM solutions using high-order quadrature.

Based on the trend seen in Figure 2, further increase in discrete direction number should reduce the discrepancy between discretized and prescribed asymmetry factor for high solid-angle splitting without phase-function normalization. It therefore is possible, with a sufficient number of discrete directions, that scattered energy and asymmetry factor could be accurately conserved without additional phase-function normalization. This is investigated in Figure 8, wherein FVM heat fluxes generated using up to 2024 discrete directions without the use of phase-function normalization are plotted versus wall location x^*. Solid-angle splitting of (16×16) for $M = 168$ and 288, (8×8) for $M = 624$ and 1088, and (4×4) for $M = 2024$ is applied to accurately conserve scattered energy. As a comparison, both reference MC solutions and FVM solutions with normalization at $M = 168$ are also plotted. Increasing discrete direction number to $M = 624$, 1088, and 2024 results in discretized asymmetry factors of $g = 0.9270$, 0.9282, and 0.9290, respectively, moving closer to the prescribed value $g = 0.93$. When corresponding FVM heat fluxes are compared to MC, it is seen that an increase in directions does reduce differences of results between MC and FVM. However, the three profiles with $M = 624$, 1088, and 2024 took 5650, 16,520, and 65,400 seconds to converge, respectively. In addition, the FVM profile using normalization with $M = 168$ and (2×2) splitting is more accurate than these extreme direction cases, and took only 497 seconds.

Figure 9 plots FVM heat fluxes, generated with and without normalization, in an optically thin $((1 - g)\tau = 0.07)$, purely scattering medium with $g = 0.9300$ in order to gauge the impact of optical thickness. MC results taken from Boulet et al. [26] are also presented for comparison. Sufficient solid-angle splitting

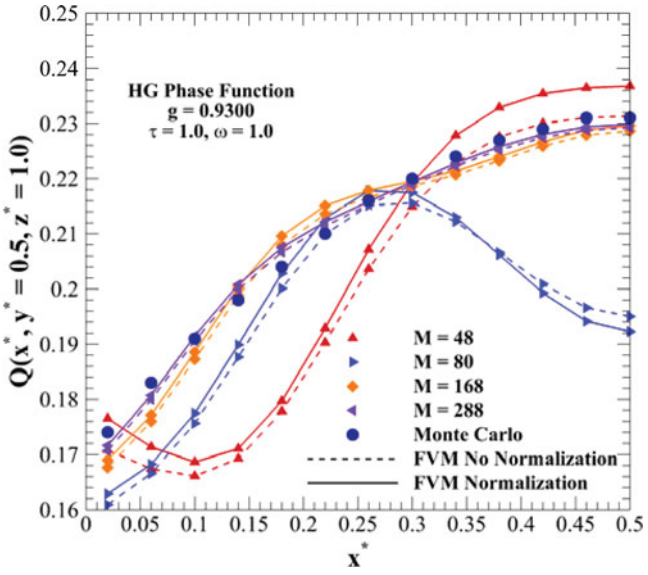

Figure 9 Impact of discrete direction number on $Q(x^*, y^* = 0.5, z^* = 1)$ and comparison with MC results [26] for $g = 0.9300$ in an optically-thin medium.

is implemented to conserve scattered energy for nonnormalized profiles, while for normalized FVM minimum (2×2) splitting is used. For the four direction numbers presented ($M = 48, 80, 168$, and 288), the difference between nonnormalized and normalized FVM heat fluxes is minimal. For an optically thin medium, radiative energy is able to penetrate a much larger distance into the medium before scattering. Therefore, fewer scattering events occur as compared to the relatively thick medium described in the rest of the analysis, and the distortions in asymmetry factor when normalization is not applied do not have as strong an impact. In addition, the FVM heat flux profiles with low-order quadrature ($M = 48$ and 80) exhibit different behavior and shape than the reference MC profiles. Physically impossible bumps in the heat flux profiles appear due to ray effect [29], an error based on angular discretization that has been shown to be prominent for optically thin media. Thus, while phase-function normalization minimizes angular false scattering errors, ray effect could be still prominent. As direction number is increased, ray effect becomes mitigated in both normalized and nonnormalized FVM results.

CONCLUSIONS

The commonly implemented technique of solid-angle splitting in the FVM is able to conserve scattered energy, provided that a sufficient splitting density is used. Nevertheless, it may not be able to preserve the phase-function asymmetry factor, leading to angular false scattering. When scattering is highly anisotropic, small deviations in asymmetry factor result in significant discrepancies in FVM radiation predictions when compared to reference MC results. Application of proper phase-function normalization eliminates errors in discretized asymmetry factor, as well as scattered energy, and produces FVM results that are more accurate to MC predictions than when normalization is ignored. While sufficient increases in discrete direction number can reduce/minimize angular false-scattering errors in FVM, use of phase-function normalization is a more effective method to improve treatment of anisotropic scattering in radiation transfer computation, as it improves computational efficiency and accuracy.

NOMENCLATURE

A_i	facial surface area of CV face i
$A^{l'l}$	normalization coefficients
D_i^l	directional weight at face i in direction l
DOM	discrete ordinates method
ERT	equation of radiation transfer
FVM	finite volume method
g	asymmetry factor
HG	Henyey–Greenstein
I	radiative intensity $(W/m^2 sr)$
L	edge length of cubic enclosure
M	total number of discrete directions
MC	Monte Carlo
N_θ, N_ϕ	number of divisions in polar and azimuthal direction
$N_{s\theta}$, $N_{s\phi}$	solid-angle subdivisions in polar and azimuthal direction
$\hat{\boldsymbol{n}}$	surface outward normal vector
P_n	the n-th order Legendre polynomial
Q	nondimensional heat flux
$\boldsymbol{r}$	position vector
r	radial location
$\boldsymbol{S}$	radiation source term
$\hat{\boldsymbol{s}}$	unit direction vector
x, y, z	Cartesian coordinates
x^*, y^*, z^*	dimensionless Cartesian coordinates

Greek Symbols

ΔA, ΔV	control volume surface area and volume (m^2, m^3)
$\Delta\Omega$	discrete solid angle (sr)
σ_a	absorption coefficient $\left(m^{-1}\right)$
σ_s	scattering coefficient $\left(m^{-1}\right)$
Φ	scattering phase function
$\tilde{\Phi}$	normalized scattering phase function
ϕ	radiation direction azimuthal angle (°)
Θ	scattering angle (°)
θ	radiation direction polar angle (°)
τ	optical thickness
ω	single scattering albedo

Subscripts

b	blackbody
HG	Henyey–Greenstein
i	control-volume face

Superscripts

$'$ radiation incident direction
l, l' radiation directions
$l'l$ from direction l' into direction l

REFERENCES

[1] Modest, M. F., *Radiative Heat Transfer*, 2nd ed., Academic Press, New York, NY, pp. 263–530, 2003.

[2] Solovjov, V. P., and Webb, B. W., An Efficient Method for Modeling Radiative Transfer in Multicomponent Gas Mixtures With Soot, *Journal of Heat Transfer*, vol. 123, pp. 450–457, 2001.

[3] Tuncer, O., Acharya, S., and Uhm, J. H., Dynamics, NOx and Flashback Characteristics of Confined Premixed Hydrogen-Enriched Methane Flames, *International Journal of Hydrogen Energy*, vol. 34, pp. 496–506, 2009.

[4] Guo, Z., and Maruyama, S., Radiative Heat Transfer in Nonhomogeneous, Nongray, and Anisotropic Scattering Media, *International Journal of Heat and Mass Transfer*, vol. 43, pp. 2325–2336, 2000.

[5] Guo, Z., Maruyama, S., and Tagawa, S., Combined Heat Transfer in Floating Growth of Large Silicon Crystals With Radiation on Diffuse and Specular Surfaces, *Journal of Crystal Growth*, vol. 194, pp. 321–330, 1998.

[6] Krishnamoorthy, G., A Comparison of Angular Discretization Strategies for Modeling Radiative Transfer in Pool Fire Simulations, *Heat Transfer Engineering*, vol. 33, pp. 1040–1051, 2012.

[7] Kukulka, D. J., and Smith, R., Development of Vipertex EHT Solar Surfaces for Enhanced Energy Transfer Applications, *Heat Transfer Engineering*, vol. 35, pp. 551–555, 2014.

[8] Hunter, B., and Guo, Z., Normalization of Various Phase Functions for Radiative Heat Transfer Analysis in a Solar Absorber Tube, *Heat Transfer Engineering*, vol. 35, pp. 791–801, 2014.

[9] Guo, Z., and Kumar, S., Discrete Ordinates Solution of Short Pulse Laser Transport in Two-Dimensional Turbid Media, *Applied Optics*, vol. 40, pp. 3156–3163, 2001.

[10] Muthukumaran, R., and Mishra, S. C., Analysis of the Transport of a Train of Short-Pulse Radiation of Gaussian Temporal Profile Through a 2-D Participating Medium, *Heat Transfer Engineering*, vol. 30, pp. 1197–1207, 2009.

[11] Mansoor, S. B., Yilbas, B. S., and Shuja, S. Z., Laser Evaporative Heating: Influence of Laser Pulse Intensity on the Cavity Formation, *Heat Transfer Engineering*, vol. 29, pp. 328–339, 2008.

[12] Sajjadi, A. Y., Mitra, K., and Guo, Z., Thermal Analysis and Experiments of Laser-Tissue Interactions: A Review, *Heat Transfer Research*, vol. 44, pp. 345–388, 2013.

[13] Raithby, G. D., and Chui, E. H., A Finite-Volume Method for Predicting a Radiant Heat Transfer in Enclosures With Participating Media, *Journal of Heat Transfer*, vol. 112, pp. 415–423, 1990.

[14] Chui, E. H., Raithby, G. D., and Hughes, P. M. J., Prediction of Radiative Transfer in Cylindrical Enclosures With the Finite Volume Method, *Journal of Thermophysics and Heat Transfer*, vol. 6, pp. 605–611, 1992.

[15] Murthy, J. Y., and Mathur, S. R., Finite Volume Method for Radiative Heat Transfer Using Unstructured Meshes, *Journal of Thermophysics and Heat Transfer*, vol. 12, pp. 313–321, 1998.

[16] Chai, J. C., Lee, H. S., and Patankar, S. V., Finite Volume Method for Radiation Heat Transfer, *Journal of Thermophysics and Heat Transfer*, vol. 8, pp. 419–425, 1994.

[17] Raithby, G. D., Discussion of the Finite-Volume Method for Radiation, and Its Application Using 3D Unstructured Meshes, *Numerical Heat Transfer Part B*, vol. 35, pp. 389–405, 1999.

[18] Chai, J. C., Hsu, P.-F., and Lam, Y. C., Three-Dimensional Transient Radiation Transfer Modeling Using the Finite-Volume Method, *Journal of Quantitative Spectroscopy and Radiative Transfer*, vol. 86, pp. 299–313, 2004.

[19] Guo, Z., and Kumar, S., Three-Dimensional Discrete Ordinates in Transient Radiation Transfer, *Journal of Thermophysics and Heat Transfer*, vol. 16, pp. 289–296, 2002.

[20] Kim, S. H., and Huh, K. Y., A New Angular Discretization Scheme of the Finite Volume Method for 3-D Radiative Heat Transfer in Absorbing, Emitting, and Anisotropically Scattering Media, *International Journal of Heat and Mass Transfer*, vol. 43, pp. 1233–1242, 2000.

[21] Kim, T. K., and Lee, H., Effect of Anisotropic Scattering on Radiative Heat Transfer in Two-Dimensional Rectangular Enclosures, *International Journal of Heat and Mass Transfer*, vol. 31, pp. 1711–1721, 1988.

[22] Hunter, B., and Guo, Z., Conservation of Asymmetry Factor in Phase Function Discretization for Radiative Transfer Analysis in Anisotropic Scattering Media, *International Journal of Heat and Mass Transfer*, vol. 55, pp. 1544–1552, 2012.

[23] Hunter, B., and Guo, Z., Phase Function Normalization for Accurate Analysis of Ultrafast Collimated Radiative Transfer, *Applied Optics*, vol. 51, pp. 2192–2201, 2012.

[24] Hunter, B., and Guo, Z., Phase-Function Normalization in 3-D Discrete-Ordinates Solution of Radiation Transfer—Part I: Conservation of Scattered Energy and Asymmetry Factor, *Numerical Heat Transfer Part B*, vol. 62, pp. 203–222, 2012.

[25] Hunter, B., and Guo, Z., Phase-Function Normalization in 3-D Discrete-Ordinates Solution of Radiative Transfer—Part II: Benchmark Comparisons, *Numerical Heat Transfer Part B*, vol. 62, pp. 223–242, 2012.

[26] Boulet, P., Collin, A., and Consalvi, J. L., On the Finite Volume Method and the Discrete Ordinates Method Regarding Radiative Heat Transfer in Acute Forward Anisotropic Scattering Media, *Journal of Quantitative Spectroscopy and Radiation transfer*, vol. 104, pp. 460–473, 2007.

[27] Hunter, B., and Guo, Z., Reduction of Angle Splitting and Computational Time for the Finite Volume Method Via Phase Function Normalization, *International Journal of Heat and Mass Transfer*, vol. 55, pp. 2449–2460, 2012.

[28] Hunter, B., and Guo, Z., Comparison Of Discrete-Ordinates Method and Finite Volume Method for Steady-State and Ultrafast Radiative Transfer Analysis in Cylindrical Coordinates, *Numerical Heat Transfer Part B*, vol. 59, pp. 339–359, 2011.

[29] Chai, J. C., Lee, H. S., and Patankar, S. V., Ray Effect and False Scattering in the Discrete Ordinates Method, *Numerical Heat Transfer Part B*, vol. 24, pp. 373–389, 1993.

Brian Hunter received his B.S. and M.S. in mechanical engineering from Florida Institute of Technology in 2008 and 2009, respectively, and received his Ph.D. in mechanical engineering from Rutgers University in May 2014, graduating at the top of his class with a 4.0 GPA (on a 4.0 scale). He has published 12 peer-reviewed articles in archival journals, with two additional articles accepted for publication. In 2011, he was awarded the prestigious SMART scholarship through ASEE/DoD, working in conjunction with Picatinny Arsenal in Dover, NJ, where he began employment in August 2014 as a mechanical engineer in the Fuze and Precision Armaments Technology Directorate.

Zhixiong Guo received his B.S., M.S., and doctorate in engineering physics from Tsinghua University, Beijing, China, in 1989, 1991, and 1995, respectively. Following several years as a researcher for KAIST in South Korea and as a research associate for Tohoku University in Japan, he entered the Polytechnic School of Engineering, New York University (NYU-Poly), in May 1999 and received his Ph.D. degree in mechanical engineering in June 2001. Then he joined the Department of Mechanical and Aerospace Engineering at Rutgers University and was promoted to full professor in July 2012. His current research interests are in laser–matter interactions, thermal and solar radiation heat transfer, and optical measurement. He has published more than 90 peer-reviewed articles in archival journals. He has supervised seven Ph.D. students to completion and eleven postdoctoral/visiting scholars. He is a fellow of the ASME and currently serves as an associate editor for *ASME Journal of Heat Transfer* and for the international journal *Heat Transfer Research*.